A BAYESIAN METHOD FOR 3D ESTIMATION OF SUBCELLULAR PARTICLE FEATURES IN MULTI-ANGLE TIRF MICROSCOPY

Liang Liang, Hongying Shen, Yingke Xu, Pietro De Camilli, Derek K. Toomre, and James S. Duncan

Yale University, New Haven, CT 06520, USA

ABSTRACT

Multi-angle total internal reflection fluorescence microscopy (MA-TIRFM) is a relatively new and powerful tool to study subcellular particles near cell membrane due to its unique illumination mechanism. We present a MAP-Bayesian method to automatically estimate features of individual particles in MA-TIRF images, including 3D positions, relative sizes, and relative amount of fluorophores. Using the MAP criterion, the optimal values of the features can be obtained by maximizing a nonlinear functional. Initial feature values are estimated by using image filters and clustering algorithms. The method is evaluated on synthetic data and results show that it has high accuracy. The result on real data from our initial experiments is also presented.

***Index Terms*—** Bayesian estimation, total internal reflection fluorescence microscopy, subcellular particle detection

1. INTRODUCTION

Total internal reflection fluorescence microscopy (TIRFM) is widely used in biological experiments to acquire images of small subcellular particles near cell membrane due to its unique illumination mechanism. Single TIRF image is just a projection of 3D volume, and therefore it can not provide 3D information. A new generation of TIRFM, multi-angle TIRFM (MA-TIRFM), can reveal the 3D information of the particles by taking 2D TIRF images at different incident angles with a very high frequency. With the advantages of the MA-TIRFM, biologists can better understand many subcellular processes, such as endocytosis and exocytosis which we are interested in. In endocytosis, e.g., clathrin mediated endocytosis (CME), surface molecules and extracellular material are selective wrapped in small pits that are finally internalized. In exocytosis, e.g., insulin regulated glucose transporter 4 (GLUT4) vesicle exocytosis, vesicles packed with receptors, enzymes or transporters undergo successive stages including vesicle tethering/docking and fusion with the plasma membrane. The study of those cellular processes has profound implications in neuroscience, virology, and diabetes research. For instance, CME is the major route for synaptic vesicle recycling in neurons that is critical for synaptic transmission [1], and it is also one of the pathways through which viruses enter cells [2]. GLUT4 is the insulin regulated glucose transporter found primarily in adipose and muscle tissues, and is responsible for insulin stimulated glucose uptake into the cell. In humans, the dysfunction of GLUT4 translocation is highly related to insulin resistance and type II diabetes [3].

Some applications of MA-TIRFM have been developed for measuring relatively large biological structures. In [4], 3D structures of microtubules are reconstructed by fitting the decay profile of MA-TIRFM to the image data with smoothness priors. In [5], shapes of secretary granules are modeled using spheres and measured using MA-TIRFM. The method in [5] can only deal with isolated granules and some important factors are not considered in estimation algorithms, including noise distributions and intensity distributions.

In this paper, we present a MAP-Bayesian method for 3D particle feature estimation using MA-TIRFM. To our best knowledge, it is the first work that uses a MAP-Bayesian framework for measuring particles with MA-TIRFM. In section 2, we describe the image formation process, and present the MAP framework for feature estimation. In section 3, we describe the simulation setup, and report the evaluation result on synthetic datasets, and show the result on real data as well.

2. METHOD

2.1. Image Formation

In TIRFM, when the incident angle of the laser beam exceeds the critical angle, total internal reflection will occur at the interface of two mediums (coverslip and specimen) with different refractive indices. In the evanescent field generated near the interface, each fluorophore is excited to emit fluorescence light, and its intensity is proportional to the intensity of the evanescent field at the fluorophore's position. Theoretically [3], the axial profile of the evanescent field can be described using an exponential decay function with parameter d, the penetration depth, determined by the incident angle and refractive indices. The fluorescence light from the 3D volume is then captured by CCD camera. EMCCD [6] is widely used in high performance microscopes because it can detect light

This work was supported in part by the Keck foundation.

with very low intensity and almost eliminate readout noise. The image I from the EMCCD camera is determined by the fluorescence image f and the noise sources. There are mainly two types of noises [6] sequentially embedded into the image. One is the shot noise that is generated in the photon collection process and follows a Poisson distribution. The other is the excess noise that is generated during the electron multiplying process, and it follows a Gaussian distribution when the number of input photon-electrons is much greater than 10 which is usually satisfied in experiments. The overall noise distribution is the convolution of the two distributions, which is very complicated. By using a set of incident angles $\{\theta_n\}_{n=1}^N$, i.e., penetration depths $\{d_n\}_{n=1}^N$, a set of 2D images $\{I_n\}_{n=1}^N$ can be obtained.

To observe the particles, proteins of interest are labeled with fluorophores. Particle diameter (50~100nm) is comparable to the lateral pixel resolution (~160nm), and the light from each particle is blurred by point spread function (PSF) [7]. As a result, the spatial distribution of the fluorescence intensities of the particles in the x-y plane can be well modeled using Gaussian mixtures.

Therefore, the fluorescence image f_n is modeled as the sum of Gaussian mixture G_n, background b_n, given by

$$f_n(x,y) = G_n(x,y) + b_n(x,y) \tag{1}$$

The background b_n is spatially and temporally smooth. The Gaussian mixture G_n has K components, i.e., $G_n = \sum_{k=1}^K G_n^{(k)}$. Each component $G_n^{(k)}$ corresponds to a particle with a feature vector $[x^{(k)}, y^{(k)}, z^{(k)}, r^{(k)}, c^{(k)}]$, given by

$$G_n^{(k)}(x,y) = a_n^{(k)} \exp\left[-\frac{(x-x^{(k)})^2 + (y-y^{(k)})^2}{2(r^{(k)})^2}\right] \tag{2}$$

Here, $(x^{(k)}, y^{(k)})$ is the position of the k^{th} particle. Since particle size is comparable to the lateral pixel resolution, $r^{(k)}$ is the relative measure of the radius. If the size of a particle is much smaller than the lateral pixel resolution, the shape of the particle's intensity profile is almost the same as that of the point spread function (PSF) which can also be well approximated by a Gaussian function [7].

$a_n^{(k)}$ is the peak intensity of fluorescence light from the particle obtained with the angle θ_n, and it is determined by the (relative) amount of fluorophores $c^{(k)}$ in the particle and the axial profile $h_n(z)$ of the evanescent field. $h_n(z)$ can be calibrated in experiments [4]. We model the calibration error as Gaussian noise with zero mean and variance $\sigma_{h_n}^2$. Therefore, we obtain

$$a_n^{(k)} = c^{(k)} h_n(z^{(k)})_{\text{real}} \tag{3}$$

$$h_n(z^{(k)})_{\text{calibrated}} = h_n(z^{(k)})_{\text{real}} + \mathcal{N}(0, \sigma_{h_n}^2) \tag{4}$$

The image I_n obtained at the angle θ_n is determined by the fluorescence image f_n and the noise sources. The probability distribution of I_n is determined by the probability distribution of the overall noise.

2.2. The MAP Framework

The goal is to find $\{x^{(k)}, y^{(k)}, z^{(k)}, r^{(k)}, c^{(k)}\}_{k=1}^K$, the feature set of the particles that maximize the posterior probability (MAP) given the image set $\{I_n\}_{n=1}^N$ and calibrated axial profiles $\{h_n\}_{n=1}^N$, i.e., maximizing the energy:

$$E = \log p\left(\{x^{(k)}, y^{(k)}, z^{(k)}, r^{(k)}, c^{(k)}\}_{k=1}^K \,\middle|\, \{I_n, h_n\}_{n=1}^N\right) \tag{5}$$

which is equivalent to maximize the energy

$$E = \log p\left(\{G_n, b_n\}_{n=1}^N, \{c^{(k)}\}_{k=1}^K \,\middle|\, \{I_n, h_n\}_{n=1}^N\right) \tag{6}$$

Since the Gaussian mixtures are parameterized by the particle features, the energy E is a function of the particle features and the background, and we also need to find the optimal background. We partition each 2D image plane to two regions: $\Omega_n = \{(x,y)\,|G_n(x,y) \geqslant \delta\}$ and its complement Ω_n^c. Here, δ is a very small constant (0.002 in experiments). To simplify the argument, we define $I_{\Omega_n} = \{I_n(x,y)\,|(x,y) \in \Omega_n\}$ and $I_{\Omega_n^c} = \{I_n(x,y)\,|(x,y) \in \Omega_n^c\}$. Also, we define G_{Ω_n}, $G_{\Omega_n^c}$, b_{Ω_n}, and $b_{\Omega_n^c}$ in a similar way. Since $G_{\Omega_n^c} \approx 0$, it can be ignored. Assuming the noises on individual pixels are statistically independent, and using Bayes rule and ignoring constant terms, the above energy can be decomposed to:

$$E = E_1 + E_2 + E_3 + E_4 + E_5 \tag{7}$$

$$E_1 = \sum_{n=1}^N \log p\left(I_{\Omega_n^c} \,\middle|\, b_{\Omega_n^c}\right) \tag{8}$$

$$E_2 = \sum_{n=1}^N \log p\left(I_{\Omega_n} \,|G_{\Omega_n}, b_{\Omega_n}\right) \tag{9}$$

$$E_3 = \sum_{n=1}^N \log p\left(b_{\Omega_n} \,\middle|\, b_{\Omega_n^c}\right) \tag{10}$$

$$E_4 = \log p\left(\{c^{(k)}\}_{k=1}^K, \{h_n\}_{n=1}^N \,\middle|\, \{G_{\Omega_n}\}_{n=1}^N\right) \tag{11}$$

$$E_5 = \log p\left(\{G_{\Omega_n}\}_{n=1}^N\right) \tag{12}$$

The analytical expression of the energy can be obtained by using the noise models in section 2.1 together with some background smoothness model. However, it is too complicated to solve. Instead, we take three steps to solve the optimization problem. In the first step, we find the initial feature set and use it to find each region $\hat{\Omega}_n \approx \Omega_n$, which will be described in section 2.3. Then we replace Ω_n with $\hat{\Omega}_n$ in relevant equations. In the second step, we find $b_{\hat{\Omega}_n^c}$ which theoretically maximizes the energy E_1. Since the background is smooth, $b_{\hat{\Omega}_n^c}$ is just the smoothed version of $I_{\hat{\Omega}_n^c}$, which can be obtained by using local smoothing algorithms. To improve accuracy, multiple image frames can be used for background estimation. In the third step, we find $\{G_{\hat{\Omega}_n}, b_{\hat{\Omega}_n}\}_{n=1}^N$ and $\{c^{(k)}\}_{k=1}^K$ which maximize the sum of the other energy

terms. The definitions of those terms are described in the following paragraphs.

The term E_2 is determined by the overall noise distribution discussed in section 2.1, and we use a Gaussian distribution to approximate it and ignore the terms that only contain the variance, which is given by

$$E_2 = -\sum_{n=1}^{N} \sum_{(x,y)\in\hat{\Omega}_n} \frac{(G_n(x,y) + b_n(x,y) - I_n(x,y))^2}{\sigma^2_{n(x,y)}} \tag{13}$$

Here, $\sigma^2_{n(x,y)} = 2\,(G_n(x,y) + b_n(x,y))$ which is the variance of the noise on the image I_n. To make this relation valid, each pixel value is divided by the product of EM gain and video chain gain [6] which can be measured or found in the user manual of the microscope. Eq.(13) is essentially a nonlinear fitting, and we need to reduce the degrees of freedom. Then, we define the background b_n in the region $\hat{\Omega}_n$ as

$$b_n(x,y) = \sum_{k=1}^{K} \omega_n^{(k)}(x,y)\beta_n^{(k)} \tag{14}$$

Here, $\beta_n^{(k)}$ is scalar variable, $\omega_n^{(k)}(x,y) \propto G_n^{(k)}(x,y)$, and $\sum_{k=1}^{K} \omega_n^{(k)}(x,y) = 1$. Roughly speaking, we assume the background under each Gaussian component $G_n^{(k)}$ is near some constant. If higher accuracy is demanded, we can use local planes to model b_n.

Since the background is smooth, $b_{\hat{\Omega}_n}$ can not be far way from $\widetilde{b}_{\hat{\Omega}_n}$ which is the background interpolated from $b_{\hat{\Omega}_n^c}$. Therefore, the term E_3 can be defined as

$$E_3 = -\sum_{n=1}^{N} \sum_{(x,y)\in\hat{\Omega}_n} \frac{\left(b_n(x,y) - \widetilde{b}_n(x,y)\right)^2}{\widetilde{\sigma}^2_{n(x,y)}} \tag{15}$$

Here, $\widetilde{b}_n(x,y)$ in the region $\hat{\Omega}_n$ is interpolated from the background b_n in the region $\hat{\Omega}_n^c$, and $\widetilde{\sigma}^2_{n(x,y)} = 2\widetilde{b}_n(x,y)$ which is an estimation of the variance. Also, we ignore the terms that only contain the variance.

The term E_4 measures how well the decay profiles fit the feature data, which is give by

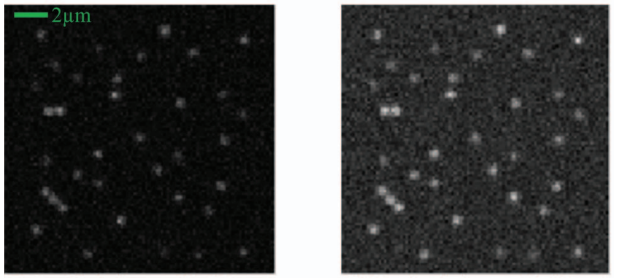
$$E_4 = -\sum_{k=1}^{K} \sum_{n=1}^{N} \frac{\left(a_n^{(k)} - c^{(k)} h_n(z^{(k)})\right)^2}{(c^{(k)}\sigma_{h_n})^2} \tag{16}$$

Assuming the features of the particles are uniformly distributed, the term E_5 is just range constraint on the features.

With the above definitions, we can find the optimal solution by using iterated conditional modes (ICM) and deterministic annealing method.

2.3. Initialization

Here we sketch a method that provides initial values of the features. First, the average value of the image set at each x-y location is calculated. The average image has higher signal to noise ratio (SNR) than a single image. Then two filters are applied to the average image, Laplacian of Gaussian (LoG) filter and Top-Hat filter. LoG filter can reveal local maxima points that are candidates of the particles. Top-Hat filter can provide supplemental information that helps to reject noise with low intensities. Therefore, each candidate point has two features from the two filters. Using a clustering algorithm [8], the points corresponding to the particles can be separated from noise points. After the initial positions are obtained, the initial values and ranges of other features can be estimated from image data. Hence, an initial feature set is obtained.



(a) Synthetic image (d=100nm) (b) Synthetic image (d=400nm)

Fig. 1. Samples of synthetic images.

3. EXPERIMENTAL RESULTS

3.1. Evaluation on Synthetic Data

The proposed method is evaluated on synthetic image datasets. Each dataset contains four images (1pixel=160nm) simulated with penetration depth 100nm, 200nm, 300nm, and 400nm as shown in Fig. 1. The particles are uniformly distributed in x-y plane. Their relative sizes are set to be the mean size obtained from real data. The SNR of the particle k is defined as $SNR = \sum_n a_n^{(k)}/\sigma^{(k)}$, and the overall noise variance is $(\sigma^{(k)})^2 = 2\sum_n \left(a_n^{(k)} + b_n(x^{(k)}, y^{(k)})\right)$. The background noise level is defined as $\lambda^{(k)} = \sigma_b^{(k)} / \left(c^{(k)} \sum_n h_n(0)\right)$, and the overall background noise variance is $(\sigma_b^{(k)})^2 = 2\sum_n b_n(x^{(k)}, y^{(k)})$. Therefore, the SNRs of individual particles can be tuned by varying the z-positions or background noise levels. To simulate the imaging process, we use the image model discussed in section 2.1.

The method is tested under different SNRs. The result is shown in Fig. 2. The root mean square errors (RMSEs) of the estimated 3D positions, the mean absolute percentage errors (MAPEs) of the estimated relative fluorophore amounts, and the MAPEs of the estimated relative radii are calculated. If higher accuracy is demanded, more penetration depths are needed to increase SNRs. We also test the method by varying the sizes of the particles while keeping the others fixed. Due to page limit, results are not shown.

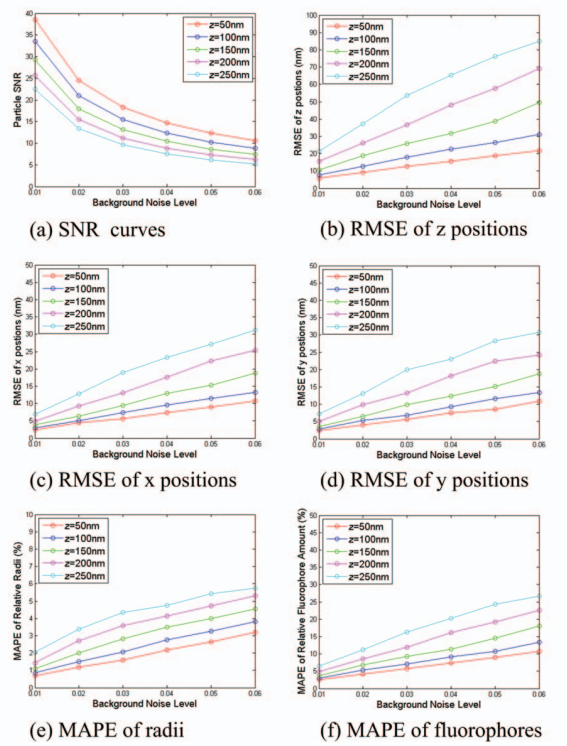


Fig. 2. Estimation result with different SNRs.

3.2. Evaluation on Real Data

To obtain the real data, mouse fibroblast cells were prepared, and clathrin coated pits are fluorescently labeled, and then images were acquired by Nikon Ti-E Eclipse inverted microscope with Apo TIRF 100× oil objective lens (NA 1.49) and Andor iXon 897 EMCCD camera. Since the acquisition rate is relatively low, we use only two angles. The first one corresponds to penetration depth $d = 64nm$, to observe the particles near the glass slide. The second one corresponds to a virtual penetration depth $d = \infty$, to observe particles in the deeper range. Although the second incident angle is greater than the critical angle, the axial profile of the light field can still be modeled as an decay function $h(z) = I_0 e^{-z/d}$ with $d = \infty$. Mathematically, it does not make any difference to the method. The result is visualized in Fig. 3.

4. CONCLUSION AND FUTURE WORK

We have proposed a MAP-Bayesian method to estimate 3D features of the particles using MA-TIRFM. We evaluate the method under different SNRs using simulation, and test it on real data. The results show the method is promising for analyzing subcellular particles.

Currently, our new MA-TIRF microscope is under calibration which is capable of taking images with a high scan rate: 50ms per angle. In the near future, we'll optimize imaging parameters and fully take advantage of the MA-TIRFM.

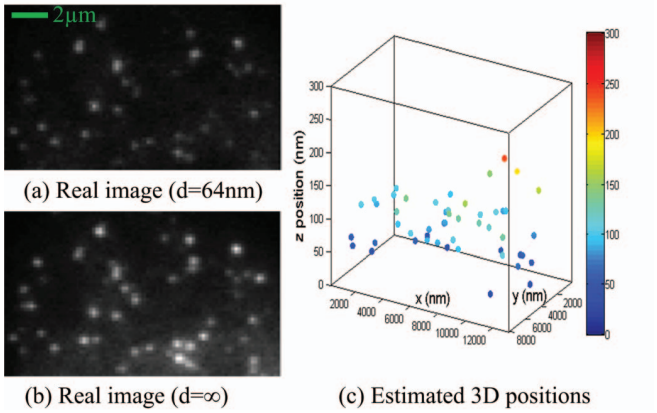


Fig. 3. Estimation result on real image samples.

5. REFERENCES

[1] V.I. Slepnev and P.D. Camilli, "Accessory factors in clathrin-dependent synaptic vesicle endocytosis," *Nature Reviews Neuroscience*, vol. 1, pp. 161–172, 2000.

[2] B. Brandenburg and X. Zhuang, "Virus trafficking - learning from single-virus tracking," *Nature Reviews Microbiology*, vol. 5, pp. 197–208, 2007.

[3] Robert T. Watson, Makoto Kanzaki, and Jeffrey E. Pessin, "Regulated membrane trafficking of the insulin-responsive glucose transporter 4 in adipocytes," *Endocrine Reviews*, vol. 25, no. 2, pp. 177–204, 2004.

[4] Q. Yang, A. Karpikov, D. Toomre, J.S. Duncan, "3D reconstruction of microtubules from multi-angle total internal reflection fluorescence microscopy using Bayesian framework," *IEEE Trans. on Image Processing*, vol. 20, no. 8, pp. 2248–2259, 2011.

[5] A. Rohrbach, "Observing secretory granules with a multiangle evanescent wave microscope," *Biophysical Journal*, vol. 78, pp. 2641–2654, 2000.

[6] M.S. Robbins and B.J. Hadwen, "The noise performance of electron multiplying charge-coupled devices," *IEEE Transactions on Electron Devices*, vol. 50, no. 5, pp. 1227–1232, 2003.

[7] B. Zhang, J. Zerubia, and J.-C. Olivo-Marin, "Gaussian approximations of fluorescence microscope point-spread function models," *Applied Optics*, vol. 46, no. 10, pp. 1819–1829, 2007.

[8] G. J. McLachlan,"Discriminant analysis and statistical pattern recognition," *New York: Wiley*, 2004.